International Journal of Solids and Structures 48 (2011) 3232–3242

Contents lists available at SciVerse ScienceDirect

International Journal of Solids and Structures

journal homepage: www.elsevier.com/locate/ijsolstr

A large deflection light-induced bending model for liquid crystal elastomers under uniform or non-uniform illumination

Lihua Jin [1], Yin Lin, Yongzhong Huo *

Department of Mechanics and Engineering Science, Fudan University, Shanghai 200433, China

ARTICLE INFO

Article history:
Received 23 March 2011
Received in revised form 5 July 2011
Available online 30 July 2011

Keywords:
Liquid crystal elastomer
Light-induced bending
Large deflection
Non-uniform illumination
Membrane force

ABSTRACT

In this paper, we propose a large deflection model for the light-induced bending of liquid crystal elastomers, in which we consider the in-plane membrane force and the geometrical nonlinearity. Based on the Hamilton principle, we derive the in-plane force balance equation and the dynamic deflection curve differential equation. The effect of light on the bending is defined as an effective optical bending moment, which is generated by the inhomogeneous light-induced strain and the membrane force. By coupling solving these two equations, we can obtain the deflection curves of LCEs under any boundary conditions and illumination. As examples, we solve the equations by an analytical-numerical method and simulate the bending under uniform illuminations. Then we consider the situations of non-uniform laser illumination and solve the equations by finite difference method. The deflection of the LCE sample can be varied and controlled by changing the illumination position, the illumination direction, the light intensity and the distribution half width of the electric field. As a result, when the LCE sample is constrained at the two boundaries, the small deflection bending theory is no longer applicable, and we need to use the large deflection theory.

1. Introduction

Liquid crystal elastomer (LCE) is a kind of crosslinked polymeric liquid crystalline solid, which combines the rubber elasticity and physical properties of liquid crystal (Warner and Terentjev, 2003). The nematic liquid crystal mesogens of LCEs have an average direction, called the director (de Gennes and Prost, 1994). When the temperature is increased to a critical value T_{ni}, the transition from the nematic phase to the isotropic phase happens, and this temperature is called the nematic–isotropic phase transition temperature. The LCE sample will contract dramatically due to the variation of the molecules' order degree.

If some photochromic liquid crystal molecules, such as azobenzenes, are added into the LCE, not only thermo but also light can induce a large contraction up to 20% (Finkelmann et al., 2001). UV light photoisomerizes the azobenzenes from the straight *trans* isomers to the bent *cis* ones, which changes the alignment and order degree of the molecules, and thus induces the large deformation, similar to the situation of thermo. Furthermore, when the light goes through the LCE sample, the light intensity decays due to the absorption, which causes the decayed light-induced deformation and thus the light-induced bending (Ikeda et al., 2003; Camacho-Lopez et al., 2004). With different molecular designs of the LCEs, different bending of the sample can be controlled (Yu et al., 2003; Tabiryan et al., 2005; Harris et al., 2005; Kondo et al., 2006; van Oosten et al., 2008; White et al., 2008, 2009; Hrozhyk et al., 2009). Thus, the photochromic LCEs have the potential applications to be remote-controllable actuators and sensors (White et al., 2008; van Oosten et al., 2009).

In recent years, photo-activated polymers have been paid a lot of attention (Finkelmann et al., 2001; Scott et al., 2005; Lendlein et al., 2005; Jiang et al., 2006). These materials share the advantage of remote control, although the mechanisms of light activation may be different. Especially, the realization of macroscopic large light-induced deformation (Finkelmann et al., 2001), different modes of light-induced bending (Yu et al., 2003; Tabiryan et al., 2005; Harris et al., 2005; Kondo et al., 2006; van Oosten et al., 2008; White et al., 2008, 2009; Hrozhyk et al., 2009) or shape memory effect (Lendlein et al., 2005; Jiang et al., 2006) makes these materials more exciting. Photomechanical models have been built up to study the light-induced behavior (Long et al., 2009; Long et al., 2011).

For the light-induced bending of LCEs, Warner and Mahadevan first derived a model under the simple beam assumption (Warner and Mahadevan, 2004). The radius of curvature under the uniform illumination is calculated. In the papers of Wei and He (2006) and He (2007), the topography of the LCE sample under the spot or

* Corresponding author. Tel.: +86 21 55664171; fax: +86 21 65642742.
E-mail addresses: lihuajin@fas.harvard.edu (L. Jin), yzhuo@fudan.edu.cn (Y. Huo).
[1] Present address: School of Engineering and Applied Sciences, Harvard University, Cambridge, MA 02138, USA.

0020-7683/$ - see front matter © 2011 Elsevier Ltd. All rights reserved.
doi:10.1016/j.ijsolstr.2011.07.015

striped illumination was simulated. Dunn (2007) calculated the curvature and deflection of the monodomain and polydomain LCE films under uniform polarized light. Considering the geometrical nonlinearity, Dunn and Maute (2009) further simulated the bending under the non-uniform illumination by the finite element method. Gaididei et al. (2010) simulated the anisotropic light-induced bending under linearly and circularly polarized light with considering the geometrical nonlinearity. Warner et al. (2010a) modeled the bending behavior with different molecular designs, and they also showed the effect that the bending in one dimension may suppress the curvature in another under certain geometry condition (Warner et al., 2010b).

However, in the previous work the effect of light on the material properties of LCE was neglected, and the light-induced strain was assumed empirically. In our previous papers (Jin et al., 2006, 2010), by considering the opto-chemical process and the nematic–isotropic phase transition, we have already introduced the light intensity into the constitutive relation, derived both Young's modulus and light-induced strain from it, and constructed a small deflection model for the light-induced bending. In this paper, we further derive a large deflection light-induced bending model, considering the membrane force and the geometrical nonlinearity. LCE samples are usually thin, and have large deflection. In the experiments, the samples are sometimes constrained at the two boundaries (Kondo et al., 2006; Cviklinski et al., 2002). Especially in a lot of designs of LCE actuators, the LCE films are under constraint, and people want to make use of the membrane force (Yamada et al., 2009; Warner et al., 2010; Wang et al., 2011; You et al., in press; Huo et al., 2011). Thus, such a large deflection model with considering membrane force and geometrical nonlinearity is essential. Based on the Hamilton principle, we derived the force balance equation and the dynamic deflection curve differential equation, in which the effect of light is defined as an effective optical bending moment, generated by the inhomogeneous light-induced strain and the membrane force. The solution of the differential equation allows us to simulate the deflection curve under any boundary conditions, and any illuminations, uniform or non-uniform, and we do not need the complicated skills, such as Hankel transform and Fourier transform (Wei and He, 2006; He, 2007). As some examples, we first calculate the deflection curves of a LCE sample under the uniform illumination and the different boundary conditions. Then we consider the non-uniform illumination of lasers, calculate the deflection curves and vary the deflection of the LCE sample by changing the illumination center, the illumination direction, the light intensity and the distribution half width of the electric field.

In Section 2, the large deflection light-induced bending model is derived based on the Hamilton principle. The solution of the deflection curve differential equation in the situation of the uniform illumination and different boundary conditions will be given in Section 3. In Section 4, we will consider the solution in the situation of non-uniform illumination and vary the deflection of the LCE samples by light controlling. The conclusions will be given in Section 5.

2. Large deflection light-induced bending model

2.1. Opto-mechanical constitutive relation

In this subsection, we will review the opto-mechanical constitutive relation (Jin et al., 2010).

The elasticity of LCE is induced by entropy. Its uniaxial stress σ-deformation λ relation could be (Bladon et al., 1994)

$$\sigma = \mu\left[\left(\frac{\lambda}{\lambda_m}\right)^2 - \frac{\lambda_m}{\lambda}\right], \tag{1}$$

where $\mu = n_s k_B T$ is the effective shear modulus dependent on the temperature T, with n_s the number of networks per unit volume. λ_m is the stress-free deformation. However, due to the light-induced deformation, λ_m changes with the light intensity I, i.e., $\lambda_m = \lambda_m(I)$. By considering the opto-chemical process and the nematic–isotropic phase transition, we can obtain $\lambda_m(I)$ and introduce the light intensity into the constitutive relation as (Finkelmann et al., 2001; Jin et al., 2010)

$$\lambda_m(I) = \begin{cases} \left(1+\alpha\left(T_{ni}^0 - T - \beta\phi(I)\right)^{\xi}\right) \Big/ \left(1+\alpha\left(T_{ni}^0 - T\right)^{\xi}\right), & \phi(I) < \left(T_{ni}^0 - T\right)/\beta, \\ 1/\left(1+\alpha\left(T_{ni}^0 - T\right)^{\xi}\right), & \phi(I) \geqslant \left(T_{ni}^0 - T\right)/\beta, \end{cases} \tag{2}$$

with choosing the configuration before illumination as the initial configuration. T_{ni}^0 is the nematic–isotropic phase transition temperature without illumination, and α, β and ξ are positive constants. $\phi = \phi(I)$ is the number fraction of the bent *cis* isomers. It is described by an approximate rate equation (Finkelmann et al., 2001; Hogan et al., 2002)

$$\frac{d\phi}{dt} = \eta_0 I(1-\phi) - \tau_{ct}^{-1}\phi, \tag{3}$$

where t is time, η_0 is the absorption constant, and $\tau_{ct} = \tau_0 \exp(\Delta/k_B T)$ is the temperature T dependent characteristic time of the thermal activated back conversion, with τ_0, Δ positive constants, and k_B the Boltzmann constant.

Due to the absorption, the light intensity decays along the light propagation. The decay can be calculated by

$$\frac{dI}{dy} = -\frac{I}{d}, \tag{4}$$

where y is the distance from the surface and d is the decay distance. When the light intensity and the concentration of chromophores are big, d depends on the fraction of *trans* isomers $1-\phi$ (Corbett and Warner, 2007; Corbett et al., 2008), and Eqs. (3) and (4) need to be solved coupling by numerical method. However, when the light intensity is large, the illumination also causes thermal effect, which is hard to distinguish from the effect of light in experiments (Jiang et al., 2010). Here for simplicity, we limit ourselves in small light intensity and low concentration of *cis*, and the absorption of light obeys Beer's law with d a constant. Solving Eq. (4), we get

$$I(y) = I_0 \exp\left(-\frac{y}{d}\right), \tag{5}$$

with I_0 the light intensity on the surface. Then, Eq. (3) is also analytically solvable, and the isothermal solution is (Finkelmann et al., 2001; Hogan et al., 2002)

$$\phi(t, I) = \frac{\tau_{ct}\eta_0 I}{1+\tau_{ct}\eta_0 I}\left(1 - \exp\left(-(1+\tau_{ct}\eta_0 I)t/\tau_{ct}\right)\right). \tag{6}$$

From Eqs. (2), (5) and (6), we can see it is the inhomogeneous light-induced deformation $\lambda_m(I(y))$ that causes the bending.

In the following, we only consider the situation of small total strain $\varepsilon^t = \lambda - 1$, and we can linearize Eq. (1) at $\lambda = 1$ as

$$\sigma = E(\varepsilon^t - \varepsilon^m), \tag{7}$$

where E is Young's modulus and ε^m is the light-induced strain

$$E(I) = \mu\left(\lambda_m(I) + \frac{2}{\lambda_m^2(I)}\right) \quad \text{and}$$
$$\varepsilon^m(I) = \left(\lambda_m(I) - \frac{1}{\lambda_m^2(I)}\right) \Big/ \left(\lambda_m(I) + \frac{2}{\lambda_m^2(I)}\right). \tag{8}$$

Both the light-induced strain ε^m and Young's modulus E depend on the light intensity I, and thus the position. The reason is that light

changes the order degree of LCEs, and thus varies its material properties. When the temperature T is close to T^0_{ni}, the effect of the inhomogeneous Young's modulus is large (Jin et al., 2010). The subtraction of the total strain and the light-induced strain is the elastic strain

$$\varepsilon^e = \varepsilon^t - \varepsilon^m. \tag{9}$$

2.2. Large deflection light-induced bending model

Since the deflection of LCEs' light-induced bending is usually large, in this subsection, we will build a large deflection beam bending model, in which we consider the in-plane membrane force, and consider the effect of bending on force balance and geometry.

As shown in Fig. 1, we consider a LCE strip, with the director in x direction. The LCE sample is under the upward perpendicular unpolarized light distribution $I_0(x)$, and the downward loading $q(x)$. Its length L is much larger than its width w and height h, satisfying $L \gg w \gg h$. The decayed light causes inhomogeneous light-induced deformation, which induces the bending in the x–y plane. Due to the incompressibility of the material, this further causes the bending in the y–z plane. However, because of the strip geometry, we neglect the bending in the y–z plane and consider the strip as a beam.

It is reasonable to assume there is no squashing between layers in the height direction, and thus the deflection at any position y equals the one in the middle plane, $v(x,y,t) = v(x,h/2,t)$. According to the plane cross section assumption, the displacement in x direction at position (x,y), $u(x,y,t)$, can be calculated as

$$u(x,y,t) = v_x(x,h/2,t)(h/2-y) + u(x,h/2,t), \tag{10}$$

where $v_x = \partial v/\partial x$. In the large deflection theory, we should consider the geometrical nonlinearity and use the nonlinear strain–displacement relation

$$\varepsilon^t_{xx}(x,y,t) = \frac{\partial u(x,y,t)}{\partial x} + \frac{1}{2}\left(\frac{\partial v(x,h/2,t)}{\partial x}\right)^2. \tag{11}$$

Taking the derivative with respect to x at both sides of Eq. (10), we obtain the distribution of the total strain in the x direction

$$\varepsilon^t_{xx}(x,y,t) = (h/2-y)v_{xx}(x,t) + \varepsilon^t_{xx}(x,h/2,t), \tag{12}$$

with $v_{xx} = \partial^2 v/\partial x^2$ the curvature. According to Eq. (10). The displacement at any position (x,y) can be expressed by the one in the middle plane $u(x,h/2,t)$ and $v(x,h/2,t)$, so in the following, we will insert Eq. (10), and use the single letter u and v representing the displacements in the middle plane.

The Lagrange functional of the LCE strip is

$$L = \frac{1}{2}\tilde{\rho}\iiint_v \left(u_t^2 + v_{xt}^2(y-h/2)^2 + v_t^2\right)dxdydz - \frac{1}{2}\iiint_v E\varepsilon^{e2}_{xx}dxdydz - \int q v dx, \tag{13}$$

where the first integral is the kinetic energy, with $u_t = \partial u/\partial t$ and $v_t = \partial v/\partial t$ velocities, $v_{xt} = \partial^2 v/\partial x\partial t$ angular velocity, and $\tilde{\rho}$ the mass density. In Eq. (13), we have already inserted Eq. (10). Due to the consideration of the in-plane displacement u for the large deflection model, we have two new terms: u_t^2, which is the kinetic energy of the middle plane displacement, and $v_{xt}^2(y-h/2)^2$, which is the effect of the rotation. The second integral is the elastic energy, with ε^e_{xx} the elastic strain in the x direction. Inserting Eqs. (9), (12) and (11) with $y = h/2$ into Eq. (13), we can see L Eq. (13) is a functional of displacements u and v. According to the Hamilton principle, we have

$$\begin{aligned}\delta\int_{t_0}^{t_1} L dt = \int_{t_0}^{t_1}\int_0^L \Bigg(&-\rho v_{tt} + \frac{h^2}{12}\rho v_{xxtt} + w\int_0^h \left[E\varepsilon^e_{xx}(y-h/2)\right]_{xx}dy \\ &- q + w v_{xx}\int_0^h E\varepsilon^e_{xx}dy\Bigg)\delta v dx dt \\ &+ w\int_{t_0}^{t_1}\int_0^L\left(-\tilde{\rho}hu_{tt} + \frac{\partial}{\partial x}\int_0^h E\varepsilon^e_{xx}dy\right)\delta u dx dt = 0.\end{aligned} \tag{14}$$

Since δu is arbitrary, we obtain the momentum balance in the x direction

$$-\tilde{\rho}hu_{tt} + \frac{\partial}{\partial x}\int_0^h E\varepsilon^e_{xx}dy = 0. \tag{15}$$

Assume the membrane force in position x is $F_x(x)$, so we have $\int_0^h E\varepsilon^e_{xx}dy = F_x(x)$. If we do not consider the elastic wave, we can neglect the dynamic term $-\tilde{\rho}hu_{tt}$, and then we have $\frac{\partial}{\partial x}\int_0^h E\varepsilon^e_{xx}dy = 0$. Thus $\int_0^h E\varepsilon^e_{xx}dy = F_x$, where F_x is independent on x. Inserting Eqs. (9), (12) and (11) with $y = h/2$ into $\int_0^h E\varepsilon^e_{xx}dy = F_x$, we obtain

$$\begin{aligned}\varepsilon^t_{xx}(x,h/2,t) &= u_x(x,t) + v_x^2(x,t)/2 \\ &= v_{xx}(x,t)(\bar{y}(x,t) - h/2) + \bar{\varepsilon}^m_{xx}(x,t) + F_x(t)/\overline{E}(x,t)h,\end{aligned} \tag{16}$$

where

$$\bar{y}(x,t) \triangleq \frac{1}{\overline{E}(x,t)h}\int_0^h E(x,y,t)y dy \quad \text{and}$$
$$\bar{\varepsilon}^m_{xx}(x,t) \triangleq \frac{1}{\overline{E}(x,t)h}\int_0^h E(x,y,t)\varepsilon^m_{xx}(x,y,t)dy, \tag{17}$$

with the effective Young's modulus $\overline{E}(x,t) \triangleq \frac{1}{h}\int_0^h E(x,y,t)dy$ at position x. ε^m_{xx} is the light-induced strain in the x direction, and $\bar{\varepsilon}^m_{xx}$ is the weighted average of the light-induced strain. Eq. (16) is a coupling differential equation for u and v, with the unknown membrane force F_x. Integrating its both sides with respect to x from 0 to L, we obtain

$$\begin{aligned}\frac{F_x(t)}{h} = E_0(t)\Bigg[&\varepsilon_0(t) - \varepsilon^m_0(t) + \frac{1}{2L}\int_0^L v_x^2(x,t)dx \\ &- \frac{1}{L}\int_0^L v_{xx}(x,t)\left(\bar{y}(x,t) - \frac{h}{2}\right)dx\Bigg],\end{aligned} \tag{18}$$

with

$$\varepsilon_0(t) = \frac{u(L,t)-u(0,t)}{L}, \quad \frac{1}{E_0(t)} = \frac{1}{L}\int_0^L \frac{dx}{\overline{E}(x,t)},$$
$$\varepsilon^m_0(t) = \frac{1}{L}\int_0^L \bar{\varepsilon}^m_{xx}(x,t)dx. \tag{19}$$

Further due to the arbitrariness of δv, we obtain the dynamic deflection curve equation

$$\begin{aligned}&\rho v_{tt}(x,t) - \frac{h^2}{12}\rho v_{xxtt}(x,t) + (\overline{D}(x,t)v_{xx}(x,t))_{xx} - wF_x(t)v_{xx}(x,t) \\ &\quad = -q(x,t) - q_{eff}(x,t),\end{aligned} \tag{20}$$

where we have already inserted Eq. (16). $\rho = wh\tilde{\rho}$ is the mass per unit length, and $\overline{D}(x,t)$ is the effective bending stiffness

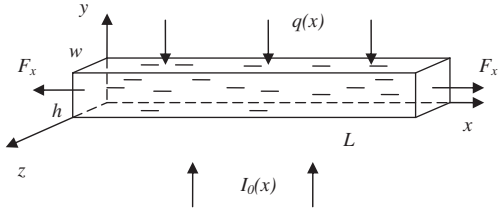

Fig. 1. Schematic of the LCE strip, with the director in x direction. It is under the upward light distribution $I_0(x)$, and the downward loading $q(x)$.

$$\overline{D}(x,t) = \overline{EI_z}(x,t) = w\int_0^h E(x,y,t)(y-\bar{y}(x,t))^2 dy. \tag{21}$$

Light produces an effective optical loading q_{eff}. q_{eff} is defined as the second derivative of the effective optical bending moment $q_{eff}(x,t) \triangleq \partial^2 M_{eff}(x,t)/\partial x^2$, where

$$\begin{aligned} M_{eff}(x,t) &\triangleq w\int_0^h E(x,y,t)\left[\varepsilon_{xx}^m(x,y,t) - \bar{\varepsilon}_{xx}^m(x,t)\right] y dy + wF_x(h/2-\bar{y}) \\ &= M_{eff}^s + M_{eff}^F. \end{aligned} \tag{22}$$

The effective optical bending moment includes two terms. The first term M_{eff}^s is caused by the non-uniform nonlinear light-induced strain, which also exists in small deflection theory (Jin et al., 2010). While the second term M_{eff}^F is the moment produced by the membrane force in the middle plane with respect to the bending axis $\bar{y}$ as defined in Eq. (17). M_{eff}^F is a new term in the large deflection model. When there is no light, we have $\varepsilon_{xx}^m = 0$ and $\bar{y} = h/2$, and thus the effective moment M_{eff} vanishes. In the deflection curve Eq. (20), the term $-\rho h^2 v_{xxtt}/12$ comes from the dynamic effect of the rotation, the term $-wF_x v_{xx}$ comes from the consideration of the effect of the large deflection bending on the geometry and balance. In the following, we only consider the quasi-static process, i.e., the very slow bending, and the first two dynamic terms in Eq. (20) can be neglected.

Eq. (20) is a fourth order ordinary differential equation of v. However, F_x is still unknown. Thus, we further need to use Eq. (16) or (18). Then with four boundary conditions of v, and one of u, we can solve both the deflection v and the membrane force F_x. We can further calculate the effective bending moment, the bending curvature, the stress and strain distribution.

3. Uniform illumination

When the illumination is uniform and no mechanical loading is applied the effective bending stiffness $\overline{D}$ and moment M_{eff} is independent on x, so the quasi-static deflection curve Eq. (20) can be reduced to

$$\overline{D}v_{xxxx} - wF_x v_{xx} = 0. \tag{23}$$

If we only consider the positive membrane force, i.e., $\lambda^2 \triangleq wF_x/\overline{D} > 0$, the general solution for Eq. (23) is

$$v = c_1 \sinh\lambda x + c_2 \cosh\lambda x + c_3 x + c_4. \tag{24}$$

We need five boundary conditions to decide $c_1 - c_4$ and F_x. In the experiments, people usually fix the LCE sample by different fixtures. Thus, in the following we will discuss the solutions under different boundary conditions respectively.

3.1. Two-end clamped boundary condition with fixed length

If the LCE sample is clamped on both ends $x = 0$ and $x = L$, and the length is fixed in the x direction, such as in paper (Kondo et al., 2006), we can use the clamped boundary condition for v and set the displacements u at the two ends are equal. The five boundary conditions are

$$v|_{x=0} = v_x|_{x=0} = v|_{x=L} = v_x|_{x=L} = 0 \quad \text{and} \quad u|_{x=L} - u|_{x=0} = 0. \tag{25}$$

Insert the boundary condition of u into Eq. (18), and the membrane force satisfies

$$\frac{F_x L}{\overline{E}h} = \left(\frac{h}{2} - \bar{y}\right)(v_x|_{x=L} - v_x|_{x=0}) + \frac{1}{2}\int_0^L v_x^2 dx - \bar{\varepsilon}_{xx}^m L. \tag{26}$$

Using the boundary conditions of v to calculate $c_1 - c_4$ in Eq. (24), we obtain $v(x) = 0$. Then according to Eq. (26), the membrane force is $F_x(t)/h = -\overline{E}(t)\bar{\varepsilon}_{xx}^m(t)$. We can see by clamping the sample on both ends, we can prevent its bending, and only a membrane force is needed to keep the initial length.

For the simulation in this paper, we choose the constants as measured in the paper of Hogan et al. (2002): $T_{ni}^0 = 340\,K, \alpha = 0.22, \xi = 0.195, \beta = 11.8\,K, \Delta = 4\times10^{-20}\,J$, and define the normalized variables $\theta \triangleq T/T_{ni}^0, i_0 \triangleq \tau_{ct}\eta_0 I_0$, where τ_{ct} is temperature dependent and with $i_{0r} \triangleq i_0(\theta = 0.88)$ at the room temperature. Fig. 2 shows the evolution of the membrane force under different light intensity $i_{0r} = 1, 3, 5$, with $\theta = 0.88$, $h/d = 1$, $L/h = 10$. F_x increases with time and light intensity, and arrives at a steady value when time is large enough, which agrees with the experiments (Kondo et al., 2006).

3.2. Two-end simply supported boundary condition with fixed length

When the fixtures of the sample can rotate freely, we consider the boundary condition of v as simply supported on both ends. With the fixing of the length, the five boundary conditions are

$$v|_{x=0} = M_{h/2}|_{x=0} = v|_{x=L} = M_{h/2}|_{x=L} = 0 \quad \text{and} \quad u|_{x=L} - u|_{x=0} = 0, \tag{27}$$

where $M_{h/2}$ is the moment with respect to the middle plane $y = h/2$, $M_{h/2} \triangleq \int_0^h E\varepsilon_{xx}^e(y-h/2)dy = -\overline{D}v_{xx} - M_{eff}$. Thus the two moment boundary conditions can be expressed by the derivative of v as

$$v_{xx}|_{x=0} = v_{xx}|_{x=L} = -M_{eff}/\overline{D}. \tag{28}$$

According to the four boundary conditions of v, we can solve the constants $c_1 - c_4$ and expressed v by the functions of the membrane force F_x

$$v = \frac{M_{eff}}{\overline{D}\lambda^2}\left(\frac{\cosh\lambda L - 1}{\sinh\lambda L}\sinh\lambda x - \cosh\lambda x + 1\right). \tag{29}$$

Inserting the boundary condition of u, Eq. (29) and its derivatives into the force balance equation (18), we obtain a nonlinear equation of F_x. We can numerically solve F_x, and thus v.

Fig. 3 shows the deflection curve of the LCE strip under upward illumination and the two-end simply supported boundary. The light intensities are $i_{0r} = 0.2, 1, 3$ respectively, and the other variables are $\theta = 0.88$, $h/d = 1$, $L/h = 10$ and $t \to \infty$. The dependence of the deflection on the light intensity is non-monotonic. The deflection first increases with the light intensity, but after a critical value

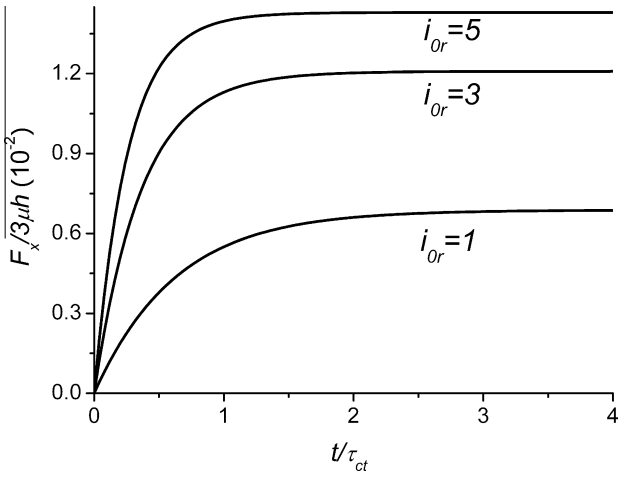

Fig. 2. The evolution of the membrane force $F_x/3\mu h$ under the two-end clamped boundary condition and the different light intensity $i_{0r} = 1, 3, 5$.

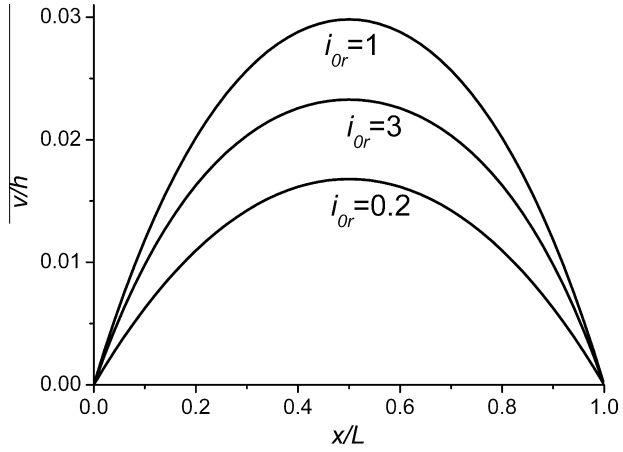

Fig. 3. The deflection curve under the two-end simply supported boundary condition and the different light intensity $i_{0r} = 0.2, 1, 3$.

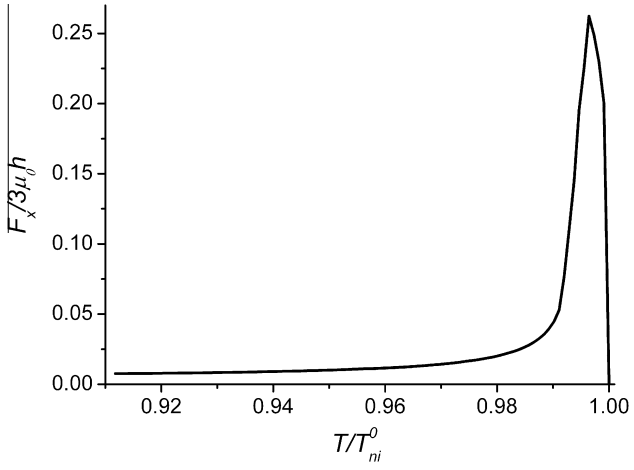

Fig. 4. Dependence of the membrane force $F_x/3\mu_0 h$ on temperature.

of the light intensity, it decreases. In the paper of Jin et al. (2010), we have the detailed discussion about the non-monotonic behaviors of the small deflection light-induced bending model. The dependence of the membrane force on the light intensity is also strongly nonlinear. Fig. 4 shows $F_x/3\mu_0 h$ versus temperature, with $\mu_0 = \mu(\theta = 0.88)$, $h/d = 1$, $L/h = 10$, $i_{0r} = 1$ and $t \to \infty$. When $T \ll T^0_{ni}$, the light-induced contraction is small, so the membrane force $F_x/3\mu_0 h$ is small. While when the temperature is close to the transition temperature T^0_{ni}, $F_x/3\mu_0 h$ dramatically increases with the temperature by about one order of magnitude, and then decreases to zero at T^0_{ni}.

The main difference between the large and small deflection theories is whether the membrane force affects the bending deflection, i.e., with or without the term $wF_x v_{xx}$ in Eq. (23). Fig. 5 compares the deflections of large and small deflection theories under temperature far from ($\theta = 0.88$) or close to ($\theta = 0.98$) the transition temperature, with $h/d = 1$, $L/h = 10$, $i_{0r} = 1$ and $t \to \infty$. The lines with solid points represent the result of the large deflection theory, while the ones with hollow points represent the small deflection theory. From the figure we can see the membrane force has large effect on the deflection. Even when the temperature is far from the transition temperature $\theta = 0.88$, the deflection calculated by the small deflection theory is larger than the large deflection theory by 85%. When $\theta = 0.98$, it is larger than the large deflection

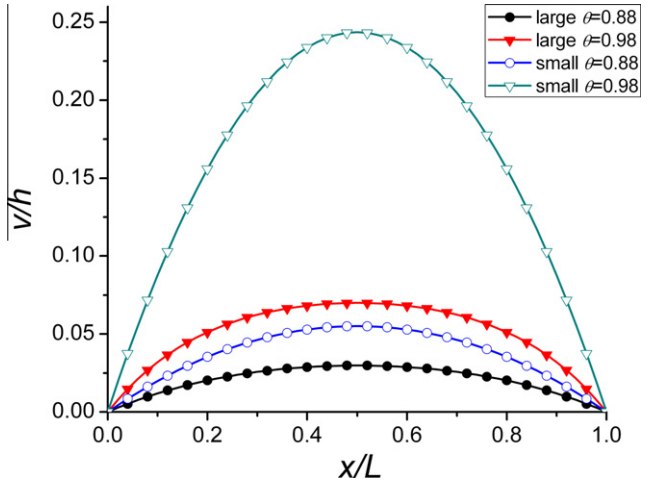

Fig. 5. Comparison of the deflection curve results based on the small and large deflection theories under different temperature $\theta = 0.88$, 0.98 and the two-end simply supported boundary condition.

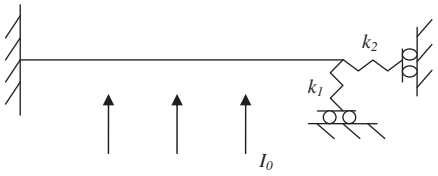

Fig. 6. Schematic of the one end clamped and the other spring boundary condition.

theory by 250%. As a conclusion, if we fix the length of the LCE sample, the small deflection bending theory is no longer applicable, due to the existence of the membrane force.

3.3. One end clamped and the other spring boundary condition

As shown in Fig. 6, if the LCE sample is clamped on one end, but fixed by springs on the other end, with the stiffness of the springs k_1 and k_2, the five boundary conditions are

$$v|_{x=0} = v_x|_{x=0} = M_{h/2}|_{x=L} = 0 \quad Q|_{x=L} = -k_1 v \quad \text{and}$$
$$wF_x = -k_2(u|_{x=L} - u|_{x=0}), \tag{30}$$

where $Q = dM_{h/2}/dx$ is the transverse force on the cross section. According to the definition of $M_{h/2}$, the transverse force boundary condition can be rewritten as

$$v_{xxx} = k_1 v/\bar{D}. \tag{31}$$

Inserting the boundary condition of u into Eq. (18), we obtain the force balance as

$$\left(\frac{L}{\bar{E}h} + \frac{w}{k_2}\right)F_x = \left(\frac{h}{2} - \bar{y}\right)(v_x|_{x=L} - v_x|_{x=0}) + \frac{1}{2}\int_0^L v_x^2 dx - \bar{\varepsilon}^m_{xx} L. \tag{32}$$

Following the similar procedures as last subsection, we can relate the constants $c_1 - c_4$ to the membrane force F_x as

$$\begin{aligned} c_1 &= \frac{M_{eff}}{\bar{D}\lambda^2}\frac{\lambda^3\sinh\lambda L - (\cosh\lambda L - 1)k_1/\bar{D}}{\lambda^3 + (\lambda L\cosh\lambda L - \sinh\lambda L)k_1/\bar{D}}, \\ c_2 &= -c_4 = \frac{M_{eff}}{\bar{D}\lambda^2}\frac{-\lambda^3\cosh\lambda L + (\sinh\lambda L - \lambda L)k_1/\bar{D}}{\lambda^3 + (\lambda L\cosh\lambda L - \sinh\lambda L)k_1/\bar{D}}, \\ c_3 &= \frac{M_{eff}}{\bar{D}\lambda}\frac{(\cosh\lambda L - 1)k_1/\bar{D} - \lambda^3\sinh\lambda L}{\lambda^3 + (\lambda L\cosh\lambda L - \sinh\lambda L)k_1/\bar{D}}. \end{aligned} \tag{33}$$

Insert v and its derivatives into the force balance equation (32), and we can numerically solve F_x and thus v.

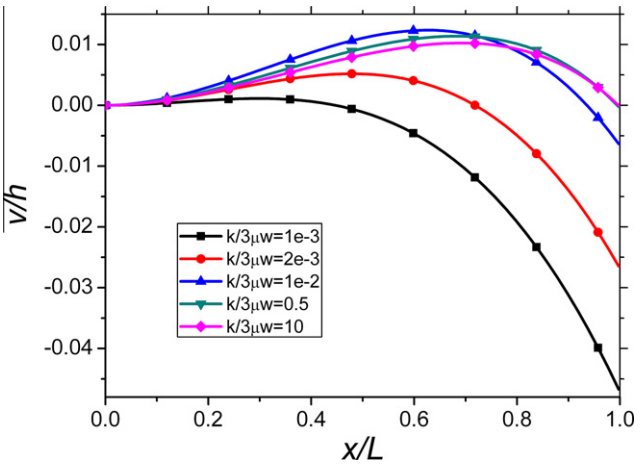

Fig. 7. The deflection curves of the LCE strip under the one end clamped and the other spring boundary condition with different spring stiffness $k/3\mu w = 1e{-}3, 2e{-}3, 1e{-}2, 0.5, 10$.

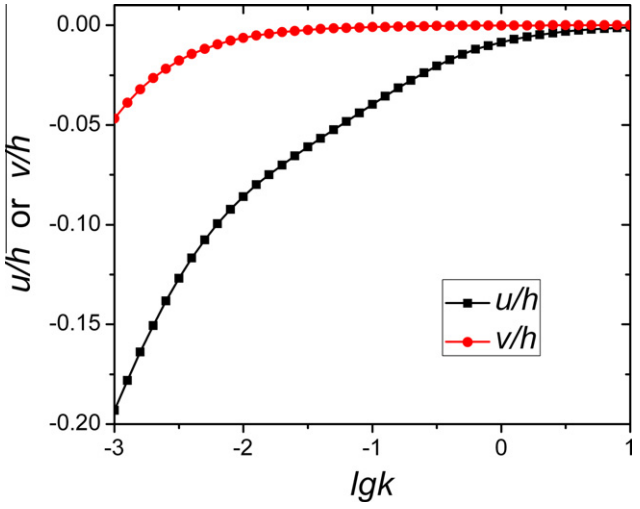

Fig. 8. The displacements of the right end u and v versus the spring stiffness.

Fig. 7 shows the deflection curve under different spring stiffness, when $k_1 = k_2 = k$, $k/3\mu w = 1e{-}3$, $2e{-}3$, $1e{-}2$, 0.5, 10, $\theta = 0.88$, $h/d = 1$, $L/h = 10$, $i_{0r} = 1$ and $t \to \infty$. When the stiffness of the spring is small, such as $k/3\mu w = 1e{-}3$, the spring k_1 has little constraint to the deflection, so the LCE sample bends downward and almost all the deflection is negative under the upward illumination as shown in Fig. 6. With the increase of k, the constraint effect of the spring k_1 becomes larger, the negative deflection of the right end becomes smaller, and the deflection of the middle part starts to be positive. When k is very large, such $k/3\mu w = 0.5$ or 10, the deflection of the right end is almost zero. Under the boundary condition of one end clamped and the other spring, besides the displacement in the y direction, the displacement in the x direction is also large. Fig. 8 shows the displacements of the right end u and v versus k, with $k_1 = k_2 = k$ and the variables same as in Fig. 7. With the increase of k, both u and v increase from the negative values to zero, while the magnitude of u is always larger than v.

4. Non-uniform illumination

In Section 3, we discuss LCEs' light-induced bending under uniform illumination. However, in real applications, non-uniform illumination is often used. In this section, we will discuss the light-induced bending of LCEs under non-uniform laser illumination. In this situation, the effective moment M_{eff}, Young's modulus and the bending stiffness are all functions of position x. Eq. (23) is no longer applicable, and we need to turn back to Eq. (20).

4.1. Effective optical bending moment

Lasers are frequently used to illuminate a LCE sample. Many lasers emit beams, with the amplitude of the electric field U satisfying a Gaussian distribution (Saleh and Teich, 1991)

$$U(r,y) = U(0,y)\exp\left(-\frac{r^2}{a(y)^2}\right), \tag{34}$$

where y is the direction of the light propagation, r is the radial distance from the center axis of the beam, and $a(y)$ is the radius at which the field amplitude drops to $1/e$ of their axial value.

Now we consider a LCE strip illuminated by a laser, as shown in Fig. 1. Because its length L is much larger than its width w and height h, $L \gg w \gg h$, we neglect the bending in the y–z plane but consider the LCE strip as a beam with bending in the x–y plane only. Since $I = U^2$, the light intensity distribution on the surface of the sample is

$$I_0(x) = I_m \exp\left(-\frac{2(x-b)^2}{a^2}\right), \tag{35}$$

where b is the illumination center ($0 \leqslant b \leqslant L$), I_m is the light intensity at $x = b$ on the surface, and $a = a(0)$ is the half width of the distribution of the electric field on the surface. Based on the light intensity distribution $I_0(x)$, we can further calculate $\varepsilon^m_{xx}(x,y,t)$, $E(x,y,t)$, $\overline{D}(x,t)$, the effective moment generated by the non-uniform nonlinear light-induced strain M^s_{eff} and the corresponding effective optical loading $q^s_{eff}(x,t) \triangleq \partial^2 M^s_{eff}(x,t)/\partial x^2$.

First we talk about the situation when the illumination center is at the middle of the LCE sample $b = 0.5L$. Fig. 9 shows the distribution of the effective moment M^s_{eff} in the x direction under laser illumination with different distribution half width of the electric field $a = 0.1L$, $0.3L$, $0.5L$. The other variables are $i_{mr} \triangleq \tau_{ct}(\theta = 0.88)\eta_0 I_m = 1$, $t \to \infty$ and $\theta = 0.88$. When the LCE sample is illuminated by lasers with the same light intensity I_m, but different distribution width of the electric field, the effective moments M^s_{eff} at the illumination center is the same. With the increase of the half width a, the width of the effective moment increases. At the same position x, the light intensity increases, and thus the effective

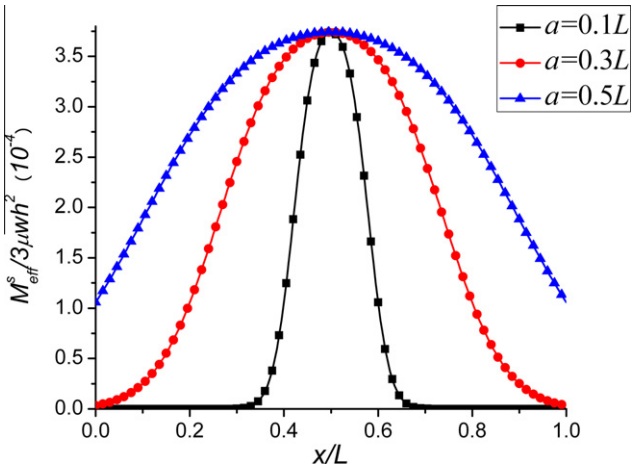

Fig. 9. The distribution of the effective moment $M^s_{eff}/3\mu wh^2$ in the x direction with different half width of the laser $a = 0.1L$, $0.3L$, $0.5L$.

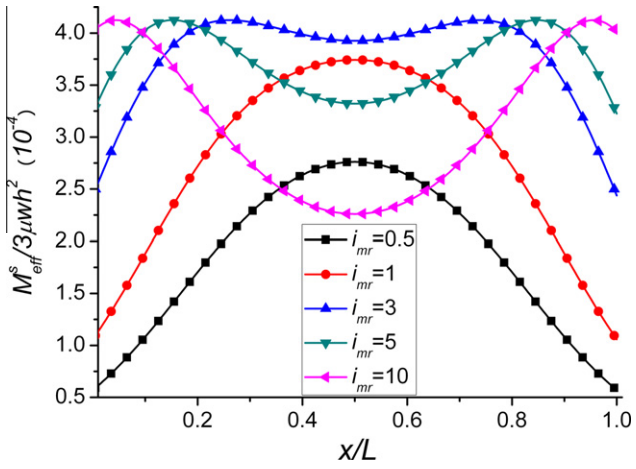

Fig. 10. The distribution of the effective moment $M^s_{eff}/3\mu wh^2$ in the x direction under different light intensity i_{mr} = 0.5, 1, 3, 5, 10.

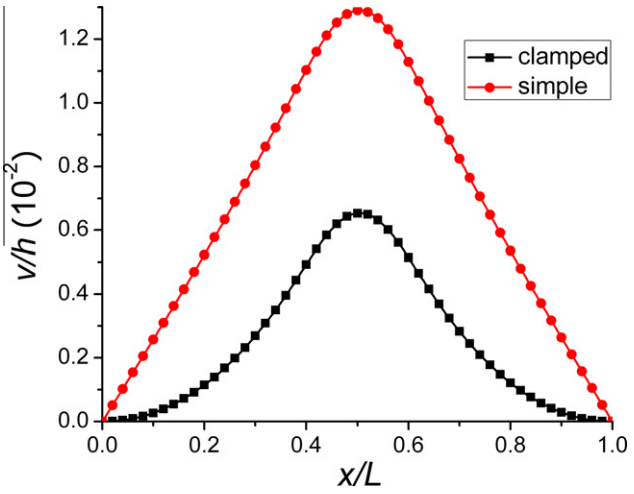

Fig. 11. The deflection curves under the two-end clamped and simply supported boundary conditions.

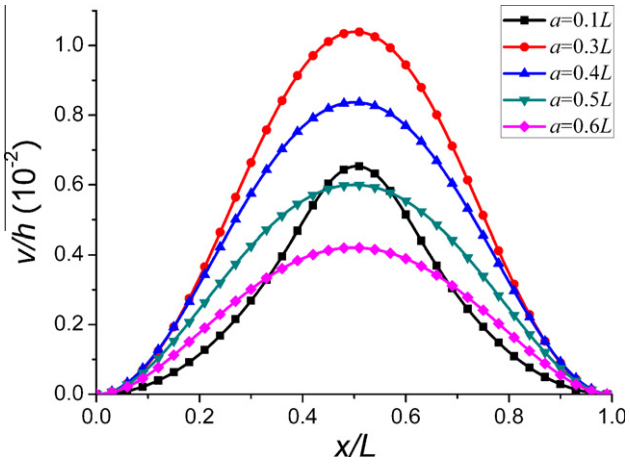

Fig. 12. The deflection curves under the two-end clamped boundary condition with different half width of the electric field a = 0.1L, 0.3L, 0.4L, 0.5L, 0.6L.

moment increases when the light intensity is not too large. However, when the light intensity is large enough, with the increase of the light intensity, the effective moment decreases. As shown in Fig. 10, when $a = 0.5L$, $t \to \infty$ and $\theta = 0.88$, under the small light intensity such as i_{mr} = 0.5, 1, the effective moment is the largest in the illumination center, but decays at the two ends. On the contrary, when the light intensity is large such as i_{mr} = 3, 5, 10, the effective moment at the illumination center is smaller than the two end regions. This non-monotonic dependence of the effective moment M^s_{eff} on light intensity can be understood as following: the increase of the light intensity only increases the light-induced strain, but not necessarily the inhomogeneity of the distribution of the light-induced strain due to the nonlinearity of the distribution of the *cis* isomers Eq. (6) and the nonlinearity of the dependence of the light-induced strain on the number fraction of *cis* isomers Eqs. (2) and (8), while it is the inhomogeneity that determines the effective moment M^s_{eff}, as shown in Eq. (22) (Jin et al., 2010). Thus it is possible that the effective moment M^s_{eff} is smaller at the position where the light intensity is bigger.

Besides M^s_{eff}, the total effective optical bending moment includes another term M^F_{eff}. M^F_{eff} is the moment produced by the membrane force in the middle plane with respect to the bending axis. Thus it is a new term due to the effect of large deflection. We can only calculate M^F_{eff} after we solve the membrane force, and we will talk about M^F_{eff} in the next subsection.

4.2. Solution of deflection curve and membrane force equations

We further need to solve the deflection curve Eq. (20) for the LCEs under non-uniform illumination. It is a fourth order nonlinear nonhomogeneous differential equation, coupled with the force balance equation (18). There is no analytical solution for this problem. We use finite difference method to coupling solve these two equations. It allows us to solve the equations under any boundary conditions and illumination.

As a result, Fig. 11 shows the deflection curves under the two-end clamped and simply supported boundary conditions, both with $i_{mr} = 1$, $a/L = 0.1$, $\theta = 0.88$, $h/d = 1$, $L/h = 10$ and $t \to \infty$. From the figure we can see the boundary condition has large effect on the bending deflection. The deflection of the two-end clamped situation is smaller than the one that is simply supported. Fig. 12 shows the deflection curves under the clamped boundary condition with different half width a = 0.1L, 0.3L, 0.4L, 0.5L, 0.6L. The other variables are $i_{mr} = 1$, $\theta = 0.88$, $h/d = 1$, $L/h = 10$ and $t \to \infty$. With the increase of the half width, the effective moment at any position increases, but due to the clamped boundary condition, the deflection may decrease. When $a \to \infty$, it is just the situation of uniform illumination as discussed in Section 3.1, and thus the deflection tends to be zero. In Fig. 10, we have already shown the distribution of the effective moment which is larger at the two ends but smaller at the illumination center. Similarly, the deflection also has non-monotonic dependence on the light intensity. Fig. 13 shows the deflection curves under the simply supported boundary condition and the different light intensity i_{mr} = 0.5, 1, 5, 20. The other variables are $a/L = 0.1$, $\theta = 0.88$, $h/d = 1$, $L/h = 10$ and $t \to \infty$. We can see with the increase of the light intensity, the deflection first increases and then decreases.

The membrane force is mainly caused by the light-induced contraction, so the boundary condition of v has little effect on the membrane force. Here we only show an example of the membrane force under the two-end clamped boundary condition. Fig. 14 is the evolution of the membrane force F_x with different half width a = 0.1L, 0.2L, 0.3L, 0.5L, and the other variables are $i_{mr} = 1$, $\theta = 0.88$, $h/d = 1$, $L/h = 10$. Since the light-induced strain increases with the illumination time, the membrane force also increases with time. With the increase of the half width a, the light-induced strain at any position x increases and the width of the light-induced strain becomes larger. According to force balance equation

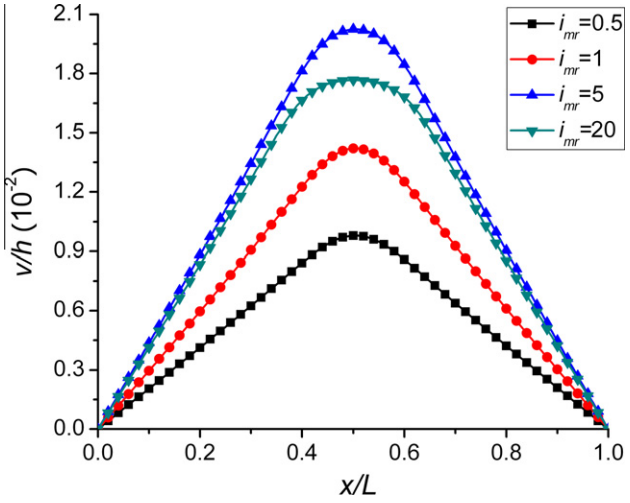

Fig. 13. The deflection curves under the two-end simply supported boundary condition and different light intensity i_{mr} = 0.5, 1, 5, 20.

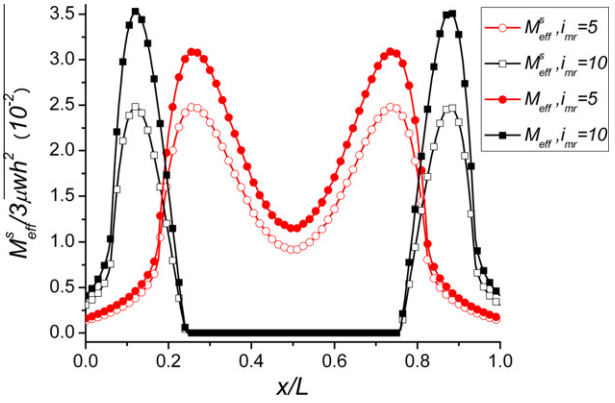

Fig. 15. The distribution of the total effective optical moment M_{eff} and the effective moment caused by the inhomogeneous light-induced strain M^s_{eff} under different light intensity i_{mr} = 5, 10.

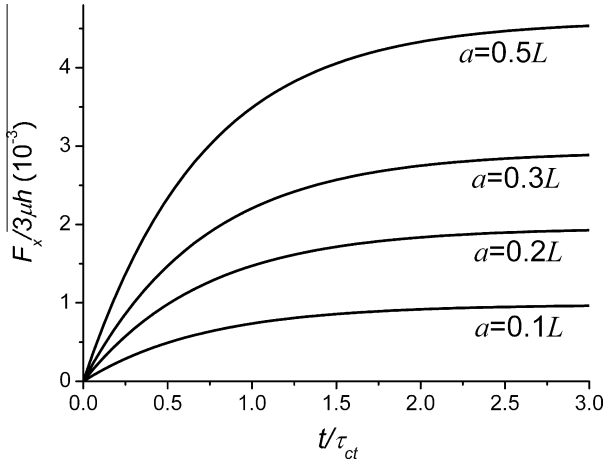

Fig. 14. The evolution of the membrane force $F_x/3\mu h$ under the two-end clamped boundary condition with different half width a = 0.1L, 0.2L, 0.3L, 0.5L.

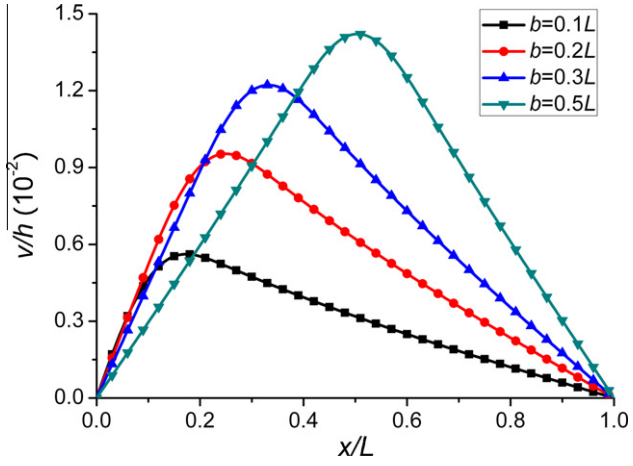

Fig. 16. The deflection curves with the different illumination position b = 0.1L, 0.2L, 0.3L, 0.5L, under the two-end simply supported boundary condition.

(18), the membrane force F_x is related to the force produced by the average light-induced strain over the whole length, so F_x monotonically increases with a.

Usually the effective moment generated by the membrane force M^F_{eff} is small, so M^s_{eff}, the effective moment generated by the inhomogeneous light-induced strain, is still the main part of M_{eff}. However, when the half width a and the light intensity I_m are large, and the temperature is close to the transition temperature T^0_{ni}, the membrane force F_x is large and the bending axis $\bar{y}$ is far from $h/2$, and thus M^F_{eff} may be large. Fig. 15 compares the difference of M_{eff} and M^s_{eff} under the large light intensity i_{mr} = 5, 10, with large half width a = 0.5L, and under high temperature θ = 0.98. The other variables are h/d = 1 and L/h = 10. The difference of M_{eff} and M^s_{eff}, i.e., M^F_{eff}, can be as large as 30% of the total effective optical bending moment M_{eff}.

4.3. Controlling LCEs' deflection

For the photochromic LCEs, the deflection can be controlled by light, which may create 3D movement (Yamada et al., 2009). In the paper of Huo et al., 2011, patterned LCE composite films were designed and bending deflection was simulated. In our model here, we can simulate the variation and controlling of the deflection of the LCE strip by changing the illumination position, the illumination direction, the light intensity, the distribution half width of the electric field and so on. Our model includes a deflection curve differential equation and a force balance equation. By these two equations, we can solve the deflection curve under any illumination, uniform or non-uniform. In this subsection, we will give some simple examples.

First let us consider the illumination position. Fig. 16 shows the deflection curves of the LCE sample under the upward laser illumination at different positions b = 0.1L, 0.2L, 0.3L, 0.5L under the two-end simply supported boundary condition. As shown in Fig. 16, when the position of the illumination center b is changed, the shape of the deflection curve varies. Since the boundary condition is symmetric, here we only discuss the situation of b < 0.5L. The other variables are a/L = 0.1, i_{mr} = 1, θ = 0.88, h/d = 1, L/h = 10 and $t \to \infty$. When the illumination center moves to the left, the position of the largest deflection moves to the left, and its magnitude decreases. The LCE sample always bends away from the light. However, when we change the boundary condition to the two-end clamped boundary condition, and keep all the other conditions, as shown in Fig. 17, the LCE sample may bend toward the light.

When we move the illumination center from the middle to the left, first, the position of the largest deflection moves to the left and the magnitude decreases, just like the situation of the simply supported boundary condition. However, when b is smaller than a critical position, the deflection starts to be negative, due to the constraint of the boundary. When $b = 0.1L$, almost all the deflection curve becomes negative.

We can also use several lasers to control the deflection of the LCE sample. As shown in Fig. 18, we simulate the deflection curve of the LCE sample under two upward laser illuminations with the two-end clamped boundary condition. The first laser is in the position $b_1 = 0.2L$, with $a_1 = 0.1L$, $i^1_{mr} = 1$, and the second laser is in the position $b_2 = 0.7L$, with $a_2 = 0.2L$, $i^2_{mr} = 1$. The other variables are $\theta = 0.88$, $h/d = 1$, $L/h = 10$ and $t \to \infty$. There are two peaks of the deflection at the two illumination centers. The second laser, which is farther to the boundary constraint and has larger half width, can cause larger deflection. Fig. 19 shows the deflection curve of a LCE sample under one upward laser and another downward laser illumination with the two-end simply supported boundary condition. The first laser is upward in the position $b_1 = 0.2L$, with $a_1 = 0.2L$, $i^1_{mr} = 1$, and the second laser is downward in the position $b_2 = 0.7L$, with $a_2 = 0.1L$, $i^2_{mr} = 2$. The other variables are the same as in Fig. 18. The two upward and downward illuminations cause a wave shape of the LCE sample, with one positive and one negative peak. However, the two peaks deviate a little from the illumination centers because of the coordination of the

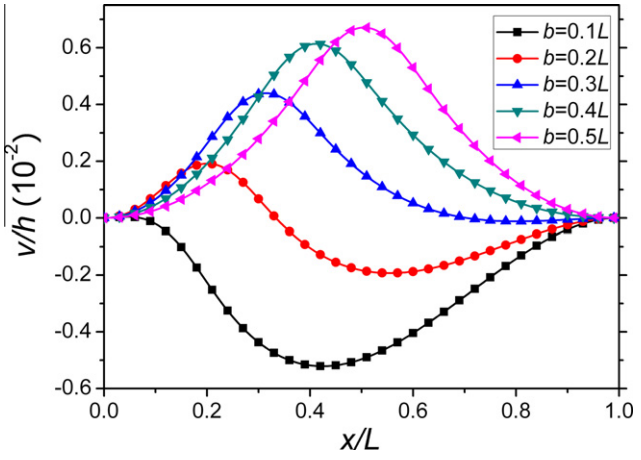

Fig. 17. The deflection curves with the different illumination position $b = 0.1L$, $0.2L$, $0.3L$, $0.4L$, $0.5L$, under the two-end clamped boundary condition.

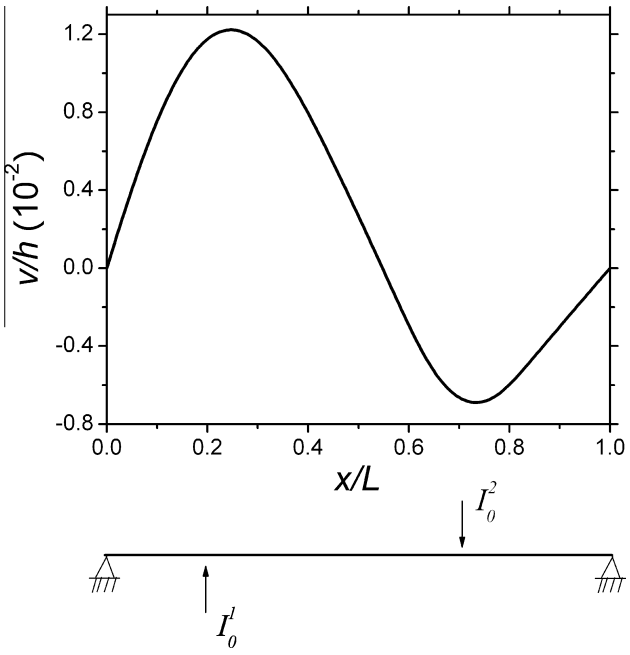

Fig. 19. The deflection curve of the LCE sample under one upward and another downward laser illuminations.

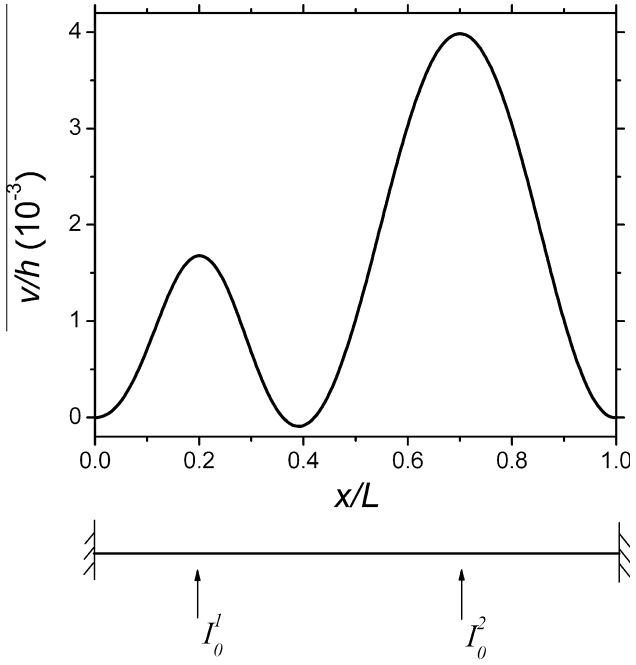

Fig. 18. The deflection curve of the LCE sample under two upward laser illuminations.

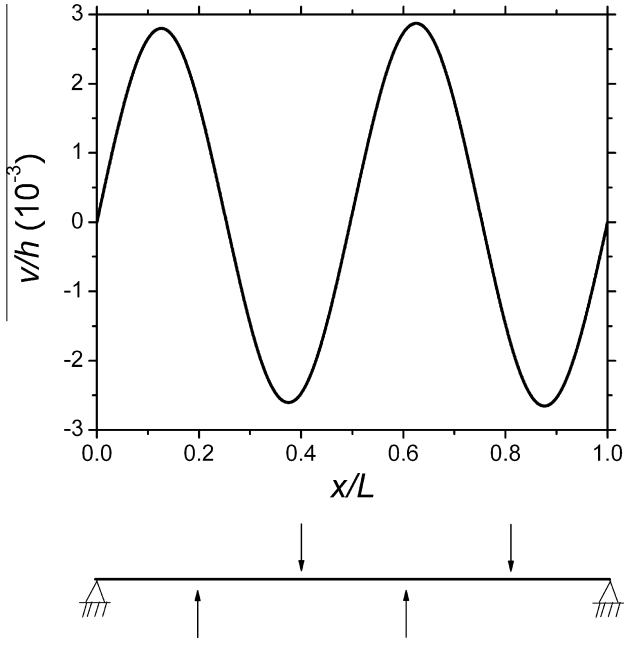

Fig. 20. The deflection curve of the LCE sample under two upward and two downward laser illuminations.

two deformations. Although the second laser has larger light intensity and is farther to the boundary, the first peak is larger, because the first illumination has larger half width, which has larger effect here.

In Fig. 20, we simulate the deflection curve of a LCE sample under two upward and two downward laser illuminations with the two-end simply supported boundary condition. The two upward lasers are in the position $b = 0.125L$ and $b = 0.625L$, i.e., the one-eighth and five-eighth of the sample, while the two downward lasers are in the position $b = 0.375L$ and $b = 0.875L$, i.e., the three-eighth and seven-eighth of the sample. All the lasers are the same with $a = 0.1L$ and $i_{mr} = 1$. The other variables are the same as in Fig. 18. The LCE sample deforms like a worm. If we can further move the illumination centers, the 'worm' can squirm.

5. Conclusions

In this paper we construct a large deflection light-induced bending model for LCEs, taking account that in the experiments the LCE sample under the illumination is always thin, has large bending deflection and is sometimes constrained at the two ends. In this model, we consider the membrane force and its effect to the bending geometry and force balance. We derive the force balance equation and the deflection curve differential equation by the Hamilton principle. The effect of light on the bending is defined as the effective optical bending moment and the effective optical loading. Calculation shows that when the light-induced contraction is constrained, the membrane force has large effect on the bending. At this time, the small deflection theory is not applicable, and we have to use the large deflection theory.

For the situation of the uniform illumination, we solve the deflection curve differential equation by an analytical-numerical method, and obtain the deflection curves under the clamped, imply supported and spring boundary conditions. As a result, the dependence of the deflection on the light intensity is non-monotonic. When the temperature is close to the transition temperature, the membrane force is much larger than the low temperature.

We further simulate the light-induced bending under the non-uniform laser illumination. We use the finite difference method to discrete the deflection curve equation, and coupling solve it with the force balance equation. The results show that the boundary conditions have large effect on the deflection. The deflection may decrease with the increase of the light intensity and the half width of the electric field. By changing the illumination position, the illumination direction, the light intensity and the half width of the electric field, we can vary the deflection of the LCE sample and control its shape. For the two-end clamped boundary condition, if we move the laser illumination from the middle to the end, the sample will change its shape from bending away from the laser to toward the laser.

However, our model is still a one-dimensional beam bending model, and it can be generalized to the two-dimensional plate bending situation. After that, we can further consider the bending under the polarized light, and simulate the controlling of the bending deflection. This will be our future work.

Acknowledgements

The authors thank the support of the National Natural Science Foundation of China (Nos. 10772049 & 11072062), and the High Technology Development Program of China (863 Program: 2009AA04Z408).

References

Bladon, P., Terentjev, E.M., Warner, M., 1994. Deformation-induced orientational transitions in liquid crystals elastomer. J. Phys. II France 4, 75–91.
Camacho-Lopez, M., Finkelmann, H., Palffy-Muhoray, P., Shelley, M., 2004. Fast liquid crystal elastomer swims into the dark. Nat. Mater. 3, 307–310.
Corbett, D., Warner, M., 2007. Linear and nonlinear photoinduced deformations of cantilevers. Phys. Rev. Lett. 99, 174302.
Corbett, D., van Oosten, C.L., Warner, M., 2008. Nonlinear dynamics of optical absorption of intense beams. Phys. Rev. A 78, 013823.
Cviklinski, J., Tajbakhsh, A.R., Terentjev, E.M., 2002. UV isomerization in nematic elastomers as a route to photo-mechanical transducer. Eur. Phys. J. E9, 427–434.
de Gennes, P.G., Prost, J.P., 1994. The Physics of Liquid Crystals. Oxford University Press, Oxford.
Dunn, M.L., 2007. Photomechanics of mono- and polydomain liquid crystal elastomer films. J. Appl. Phys. 102, 013506.
Dunn, M.L., Maute, K., 2009. Photomechanics of blanket and patterned liquid crystal elastomer films. Mech. Mater. 41, 1083–1089.
Finkelmann, H., Nishikawa, E., Pereira, G.G., Warner, M., 2001. A new opto-mechanical effect in solids. Phys. Rev. Lett. 87, 015501.
Gaididei, Y.B., Krekhov, A.P., Büttner, H., 2010. Nonlinear bending of molecular films by polarized light. Phys. Lett. A 374, 2156–2162.
Harris, K.D., Cuypers, R., Scheibe, P., Oosten, C.L., Bastiaansen, C.W.M., Lub, J., Broer, D.J., 2005. Large amplitude light-induced motion in high elastic modulus polymer actuators. J. Mat. Chem. 15, 5043–5048.
He, L.H., 2007. Surface deformation of nematic elastomers under striped illumination. Phys. Rev. E 75, 041702.
Hogan, P.M., Tajbakhsh, A.R., Terentjev, E.M., 2002. UV manipulation of order and macroscopic shape in nematic elastomers. Phys. Rev. E 65, 041720.
Hrozhyk, U., Serak, S., Tabiryan, N., White, T.J., Bunning, T.J., 2009. Bidirectional photoresponse of surface pretreated azobenzene liquid crystal polymer networks. Opt. Express 17, 716–722.
Huo, Y., You, Y., Xu, C., Lin, Y., 2011. Opto-mechanical behavior of photochromic liquid crystal polymer film composites. In: Ounaies, Z., Seelecke, S.S. (Eds.), Behavior and Mechanics of Multifunctional Materials and Composites 2011. SPIE, pp. 79780H.
Ikeda, T., Nakano, M., Yu, Y., 2003. Anisotropic bending and unbending behavior of azobenzene liquid-crystalline gels by light exposure. Adv. Mater. 15, 201–205.
Jiang, H., Kelch, S., Lendlein, A., 2006. Polymers move in response to light. Adv. Mater. 18, 1471–1475.
Jiang, X., Zhang, T., Ding, S., Huo, Y., 2010. Effect of self-heating on photo-mechanical behavior of nematic elastomers. Thermochim. Acta 500, 44–50.
Jin, L., Jiang, X., Huo, Y., 2006. Light-induced nonhomogeneity and gradient bending in photochromic liquid crystal elastomers. Sci. China Ser. G-Phys. Mech. Astron. 49, 553–563.
Jin, L., Yan, Y., Huo, Y., 2010. A gradient model of light-induced bending in photochromic liquid crystal elastomer and its nonlinear behaviors. Int. J. Nonlinear Mech. 45, 370–381.
Kondo, M., Yu, Y., Ikeda, T., 2006. How does the initial alignment of mesogens affect the photoinduced bending behavior of liquid-crystalline elastomers. Angew. Chem. 118, 1406–1410.
Lendlein, A., Hongyan, J., Junger, O., Langer, R., 2005. Light-induced shape-memory polymers. Nature 434, 879–882.
Long, K.N., Scott, T.F., Qi, H.J., Bowman, C.N., Dunn, M.L., 2009. Photomechanics of light activated polymers. J. Mech. Phys. Solids 57, 1103–1121.
Long, K.N., Scott, T.F., Dunn, M.L., Qi, H.J., 2011. Photo-induced deformation of active polymer films: single spot irradiation. Int. J. Solids Struct. 48, 2089–2101.
Saleh, B.E.A., Teich, M.C., 1991. Fundamentals of Photonics. John Wiley & Sons, New York.
Scott, T.F., Schneider, A.D., Cook, W.D., Bowman, C.N., 2005. Photoinduced plasticity in crosslinked polymers. Science 308, 1615–1617.
Tabiryan, N., Serak, S., Dai, X., 2005. Polymer film with optically controlled form and actuation. Opt. Express 13, 7442–7448.
van Oosten, C.L., Corbett, D., Davies, D., Warner, M., Bastiaansen, C.W.M., Broer, D.J., 2008. Bending dynamics and directionality reversal in liquid crystal network photoactuators. Macromolecules 41, 8592–8596.
van Oosten, C.L., Bastiaansen, C.W.M., Broer, D.J., 2009. Printed artificial cilia from liquid-crystal network actuators modularly driven by light. Nat. Mater. 8, 677–682.
Wang, B., You, Y., Huo, Y., 2011. Opto-thermo actuation of multilayered liquid crystal polymer film. Thin Solid Films 519, 5310–5313.
Warner, M., Terentjev, E.M., 2003. Liquid Crystal Elastomers. Clarendon Press, Oxford.
Warner, M., Mahadevan, L., 2004. Photo-induced deformations of beams, plates and films. Phys. Rev. Lett. 92, 134302.
Warner, M., Modes, C.D., Corbett, D., 2010a. Curvature in nematic elastica responding to light and heat. Proc. R. Soc. A 466, 2975–2989.
Warner, M., Modes, C.D., Corbett, D., 2010b. Suppression of curvature in nematic elastica. Proc. R. Soc. A 466, 3561–3578.
Wei, Z.Y., He, L.H., 2006. Surface topography and its transition of nematic elastomers due to photoinduced deformation. J. Chem. Phys. 124, 064708.
White, T.J., Tabiryan, N.V., Serak, S.V., Hrozhyk, U.A., Tondiglia, V.P., Koerner, H., Vaia, R.A., Bunning, T.J., 2008. A high frequency photodriven polymer oscillator. Soft Matter 4, 1796–1798.

White, T.J., Serak, S.V., Tabiryan, N.V., Vaia, R.A., Bunning, T.J., 2009. Polarization-controlled, photodriven bending in monodomain liquid crystal elastomer cantilevers. J. Mater. Chem. 19, 1080–1085.

Yamada, M., Kondo, M., Miyasato, R., Naka, Y., Mamiya, J., Kinoshita, M., Shishido, A., Yu, Y.L., Barrett, C.J., Ikeda, T., 2009. Photomobile polymer materials—various three-dimensional movements. J. Mater. Chem. 19, 60–62.

You, Y., Xu, C., Wang, B., Jin, L., Huo, Y., in press. Photo-actuated bending of chromatic liquid crystal polymer strips and laminates. Int. J. Smart Nano Mater.

Yu, Y., Nakano, M., Ikeda, T., 2003. Directed bending of a polymer film by light. Nature 425, 145.